Annals of Nuclear Energy 155 (2021) 108144

Contents lists available at ScienceDirect

Annals of Nuclear Energy

journal homepage: www.elsevier.com/locate/anucene

Steady-state neutronic measurements and comprehensive numerical analysis for the BME training reactor

A.Sz. Ványi [a,*], B. Babcsány [a], Z.I. Böröczki [a], A. Horváth [a], M. Hursin [b,c], M. Szieberth [a], Sz. Czifrus [a]

[a] Institute of Nuclear Techniques of Budapest University of Technology and Economics, Hungary
[b] Laboratory for Reactor Physics and Systems Behaviour of École Polytechnique Fédérale de Lausanne, Switzerland
[c] Paul Scherrer Institute, Switzerland

ARTICLE INFO

Article history:
Received 20 October 2020
Received in revised form 23 December 2020
Accepted 6 January 2021
Available online 18 February 2021

Keywords:
Reactor physics
Measurement
Validation
Diffusion
Benchmark
Steady-state
Research reactor

ABSTRACT

This paper describes steady-state reactor physics measurements and calculations that were performed for the Training Reactor of Budapest University of Technology and Economics (BME TR) with the purpose of benchmarking. Based on the available geometry specifications and material compositions a model of BME TR was created with the well-validated, general-purpose Serpent 2 Monte Carlo code. Uncertain parameters (such as fuel density and control rod positions) were adjusted to related measurements. The Serpent 2 model was used for the generation of group constants, examining several homogenization schemes. Models were created in the PARCS diffusion code, the SPNDYN diffusion and SP3 code and the PARTISN discrete ordinates code. Various Monte Carlo and deterministic calculations were performed with the adjusted models and the results were then compared with actual measured data. The calculations and measurements show good agreement, this way the Serpent model was successfully validated, while the deterministic models make a good basis for more complex benchmarks in the future, such as transients with thermal–hydraulic feedback.

1. Introduction

The comprehensive numerical analysis of nuclear reactors involves several disciplines such as reactor physics, thermal–hydraulics, thermal mechanics, material science, etc. In the past each of these aspects were treated separately by standalone single-physics codes, some of which were loosely coupled (Rhoades and Childs, 1991; Grundmann and Rohde, 1996). In the 21st century, motivated by safety purposes and helped by the ever increasing computational capacity, a new multi-physics approach is being realized in numerical reactor analysis. Novel multi-physics codes include several tightly coupled single-physics solvers within the same framework, which ensures that high resolution, high fidelity results can be obtained. Nowadays numerous novel multi-physics reactor analysis codes exist, such as the MOOSE project of Idaho National Laboratory (Gaston et al., 2009), GeN-Foam of École Polytechnique Fédérale de Lausanne (Fiorina et al., 2015) or VERA of the Consortium for Advanced Simulation of Light Water Reactors (Schmidt et al., 2015). On the other hand, the number of relevant and accessible validation measurements is low. Such a lack is essentially due to the fact that there are only a few appropriate and available reactors for this purpose. In fact, most of the research reactors are low power facilities and, therefore, they are often not suitable for the measurement of thermal–hydraulic feedback. Commercial power reactors, research reactors designed for isotope production and materials testing reactors are generally not available for such measurements. The Training Reactor of Budapest University of Technology and Economics (BME TR) is a pool-type reactor of 100 kW thermal power, which ensures accessibility for instrumentation and its power is sufficiently high to produce measurable thermal–hydraulic feedback in response to reactor physics transients. Thus, BME TR is a suitable facility for designing and performing code validation measurements. This paper is about the first set of such experiments focusing on static neutronic measurements and reactor physics modeling of BME TR. Section 2 presents the main parameters of the reactor and the known inaccuracies regarding the geometry and the material compositions. Section 3 describes the measurements performed. Section 4 and 5 briefly introduce the used methods and the computer codes as well as the developed reactor physics models. Finally, the comparison between measurements and calculations is reported in Section 6.

* Corresponding author.
E-mail address: vanyi.andras@reak.bme.hu (A.Sz. Ványi).

https://doi.org/10.1016/j.anucene.2021.108144
0306-4549/

2. BME training reactor

The Training Reactor of BME is a light water moderated and cooled pool-type reactor. The facility is located at the Central Campus of BME. The construction of the reactor started in 1966 and it was commissioned in 1971. The initial maximum reactor thermal power was 10 kW, which was increased to 100 kW in 1980 by the insertion of a fresh fuel assembly into the core. The main purpose of the facility is to train engineers and physicists. In addition to that, ever since its commission, BME TR has also been a center of scientific research and industrial project development.

The reactor core is located at the bottom of a cylindrical vessel, which has a height of 6 m and a diameter of 1.4 m (see Figs. 1 and 2). The core consists of 24 elements of regular (i.e. containing 16 fuel pins in a regular rectangular lattice) and modified (i.e. either the number of pins is reduced or the lattice is irregular) EK-10 fuel assemblies, which contain nominally 10% enriched UO_2 in metal magnesium matrix. The fuel assemblies are surrounded by 41 elements of solid graphite reflector blocks. The vessel is filled with demineralized water. All structural components inside the tank (such as fuel rod and assembly cladding, control rod guide tubes, etc.) are made of an aluminum alloy containing more than 99.5% Al.

The reactor accommodates several vertical dry and wet irradiation channels, five horizontal beam tubes, a large irradiation tunnel and a pneumatic rabbit system with three branches. The startup of the reactor is assisted by a conventional plutonium-beryllium neutron source.

The criticality control of BME TR is ensured by two safety and two control rods:

- Safety rod 1 (abbreviation: SR1) is located between the fuel assemblies E6 and F5, containing B_4C pellets;
- Safety rod 2 (abbreviation: SR2) is located between the fuel assemblies D5 and E4, containing B_4C pellets;
- Manual control rod (abbreviation: MAN) is located between the fuel assemblies C6 and D5, containing B_4C, controlled manually;
- Automatic control rod (abbreviation: AUT) is located between the fuel assemblies C4 and D3; it consists of a stainless steel tube covered by a thin cadmium layer. This rod can be operated both manually and in automatic mode by the control unit.

Rod positions are given in millimeters: $z = 0$ mm corresponds to the fully inserted state, while $z = 600$ mm to the completely withdrawn state.

The reactor can be operated in two modes. In manual mode, the operator assumes full control of the absorber rods, while in automatic mode the central control unit keeps the reactor critical by continuously adjusting the automatic control rod level to the critical position.

According to operating rules, during operation the temperature of the coolant in the primary circuit must be between 20 °C and 60 °C. The moderator can be cooled by the secondary loop or heated by an electrical heater.

The reactor has not been refueled since its initial commissioning. Based on operation logs, the released thermal energy is approximately 18.8 MWdays, which corresponds to an average burnup of 0.7 MWd/kgU for the fuel.

2.1. Known uncertainties

The reactor was built in the late 1960s. All of its components, except for the fuel, were fabricated in Hungary, while the fuel was of Soviet origin. At that time, the construction of nuclear reactors and the production technology of nuclear fuel were still in an

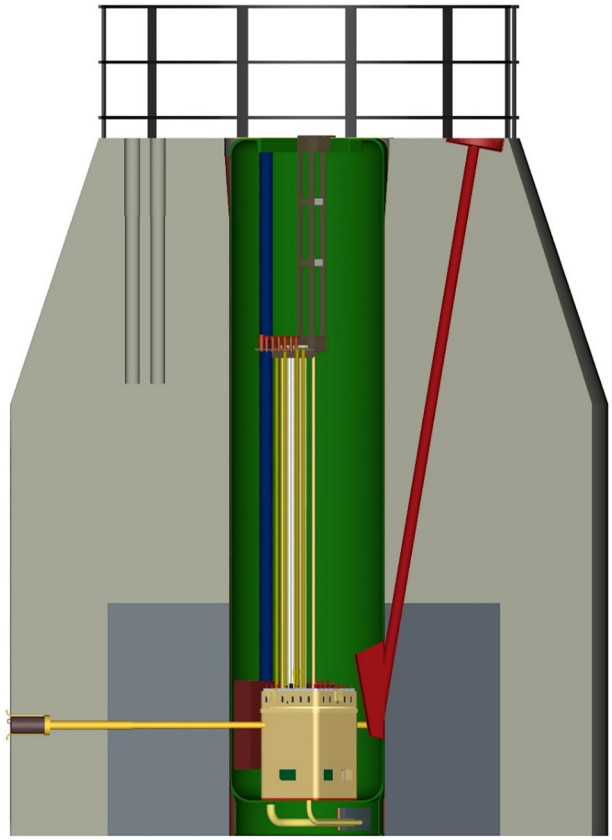

Fig. 1. CAD illustration of the BME TR reactor core, vessel and concrete shielding (Csom et al., 2020).

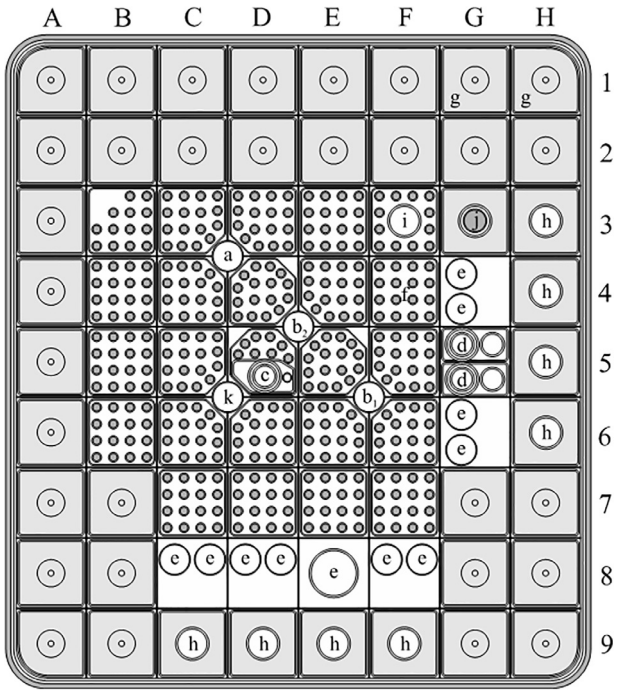

Fig. 2. Layout of BME TR core: *a* – automatic control rod (AUT); b_1, b_2 – safety rods (SR1, SR2); *c* – "fast" pneumatic rabbit; *d* –, "thermal" pneumatic rabbit; *e* – vertical irradiation channels in water; *f* – fuel assemblies; *g* – graphite reflector elements; *h* – vertical irradiation channels in graphite; *i* – vertical irradiation channels in fuel assemblies; *j* – neutron source; *k* – manual control rod (MAN) (Szatmáry and Horváth, 2018).

early phase (the first Hungarian research reactor (today: Budapest Research Reactor (Budapest Neutron Centre, 2020)) was commissioned in 1959). Thus, the documentations of certain reactor components were not sufficiently detailed and uncertainties of some important quantities (e.g. fuel enrichment) are relatively high compared to the requirements of the 21st century. The rest of this section describes all the known significant uncertainties regarding the reactor geometry structure and its material compositions.

2.1.1. Nuclear fuel

Fig. 3 shows the structure and the physical dimensions of the fuel pins according to the original documentation. Measurements on spare rods, that were fabricated a decade later in the 1970s showed asymmetric pins with varying end plug dimensions. Underwater video camera tapes confirmed that the variation of rod lengths can be as much as 5–10 mm. According to preliminary calculations the integrated effect of the fuel rod length deviation is not significant in terms of the multiplication factor.

The lattice parameters of the regular assemblies are well known; however, the structure of the modified assemblies was poorly documented. These were reconstructed using the available logs and the precise technical drawings of the regular assemblies (Szatmáry and Horváth, 2018).

Table 1 contains the documented composition of the fresh fuel in grams per fuel rod. The uncertainty of the U-235 enrichment is ±0.2 w/w%, which is rather significant. The U-234 content value in Table 1 is based on previous calculations and accounts for about 150 pcm of the value of the multiplication factor (Szatmáry and Horváth, 2018).

Although the mentioned 0.7 MWd/kg burnup is quite a low value, the current material composition of the reactor was calculated with the Serpent 2 Monte Carlo code using the written operating history logs of the reactor. In this calculation, the reactor core was burnt for the periods of 1971–1980 and 1981–2020 with the corresponding average power determined from the released thermal energy.

2.1.2. Control rods

There is limited description available on the safety and control rods. It is known that the SR rods consist of boron carbide pellets, the MAN rod is also made of B_4C pellets but with smaller diameter, while the AUT rod consists of a steel tube covered by a thin layer of cadmium. The density of the boron carbide used for the pellets is known to be 1.68 g/cm^3 according to the personnel involved in the fabrication. In the recent years the spare AUT and SR rods underwent X-ray imaging, which confirmed the assumed structure and provided initial diameter values for the modeling of the rods. However, with respect to the manufacturing techniques at the time the rods were fabricated, for the modelling of the actually used rods it is not advisable to strictly follow the dimensions obtained from the imaging of the spare rods. The control rod absorber dimensions were determined by rod worth measurements and Serpent 2 calculations.

3. Measurements

The measurements described below were carried out on different periods between 2014 and 2020. Due to a reactor reconstruction in this period, the change in the burnup of the fuel was negligible between the measurements. This section describes the course and methodology of the measurements performed, while the measured data are presented in Section 6.

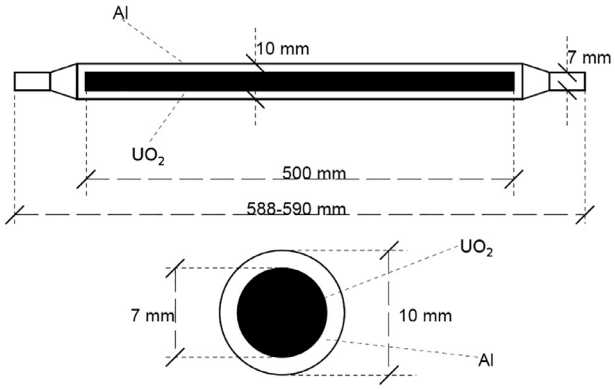

Fig. 3. Fuel rod structure and dimensions (Csom et al., 2020).

Table 1
Fresh fuel composition of a fuel pin (Szatmáry and Horváth, 2018).

Nuclide	Mass
U-235	8 g
U-238	71.936 g
U-234	0.0636 g
Mg	13.029 g
C	0.37 g
O[a]	0.42 g
B	6 ppm

[a] Oxygen that is not part of UO_2

3.1. Integral rod worth

The integral rod worth measurements for each of the two safety and two control rods were carried out by the rod drop method (Duderstadt and Hamilton, 1976). During the measurements, a LND 23210 boron-lined, argon-filled proportional counter (LND 23210, 2020) was placed in a vertical irradiation channel, connected to the irradiation tunnel. According to the manufacturer's documentation, the wall of the detector was lined with 96% enriched ^{10}B with a surface density of 0.5 mg/cm^2. The dead time of the detector was previously determined as 17 μs. The measured data were collected by the GENIE program with a measurement time of 0.2 s per channel.

For the measurements of the worth of the safety rods, the power was set to 0.2 W ($z_{MAN} = 600$ mm, $z_{AUT} = 179$ mm) and operated in this state for 15 minutes so that the delayed-neutron precursor nuclei would reach their equilibrium concentration. Then the reactor was switched to manual mode and the automatic rod was moved to 300 mm. As a result, the reactor power started to increase with a doubling time of 43 seconds. At 1.3 W the operator dropped the measured safety rod and waited a few minutes for the power to decrease. The same methodology was applied to the control rod measurements with the supercritical rod states being $z_{AUT} = 600$ mm, $z_{MAN} = 400$ mm for the automatic and $z_{AUT} = 300$ mm, $z_{MAN} = 600$ mm for the manual rod.

The reactivity for the subcritical and the supercritical states was calculated with the method of inverse kinetics:

$$\frac{\rho(t)}{\beta_{\text{eff}}} = 1 + \frac{\frac{\Lambda}{\beta_{\text{eff}}}\frac{\mathrm{d}\varphi(t)}{\mathrm{d}t} - \sum_{i=1}^{6}\frac{\beta_i}{\beta_{\text{eff}}}\lambda_i \int_{-\infty}^{t}\varphi(t')e^{-\lambda_i(t-t')}\mathrm{d}t'}{\varphi(t)} \quad (1)$$

where Λ is the generation time, β_i and λ_i are the delayed neutron fractions and decay constants, φ is the detector count.

3.2. Fuel and graphite assembly worth

Assembly worth measurements were performed for four fuel assemblies (B3, B4, C3, C4) and four graphite reflector blocks (B2, C2, D2, E2). The applied methodology is similar to that used for the control rod worth measurements. At the beginning of each measurement, the reactor power was set to 0.2 W and the MAN rod was fixed at 400 mm. The operator then raised the height of the MAN rod to 420 mm, as a result of which the power started to increase exponentially with a doubling time of about 60 seconds. At 1.2 W thermal power the given assembly was removed from the core, therefore the power decreased exponentially. The counts were registered by the aforementioned LND 23210 type neutron counter. The reactivity values for the subcritical and the supercritical states were again calculated by the method of inverse kinetics.

3.3. Relative thermal flux distribution

Relative axial flux measurements were carried out with an activation method using a Dy(5%)-Al alloy wire. From the point of view of the activation, only the radiative capture reaction of Dy-164 is relevant. The cross-section of this reaction is approximately 1/v for thermal energies and decreases quickly for neutron energies larger than 1 eV. Although several resonances can be found between 10^2 eV and 10^4 eV, over 99% of the activation in a thermal reactor is caused by neutrons with energies below the cadmium cutoff (about 0.5 eV). The reaction chain of Dy-164 is the following:

$$^{164}\mathrm{Dy} \xrightarrow{n,\gamma} {}^{165m}\mathrm{Dy} \xrightarrow{\gamma(1.3\,\mathrm{min})} {}^{165}\mathrm{Dy} \xrightarrow{\beta^-(2.35\mathrm{h})} {}^{165}\mathrm{Ho} \tag{2}$$

Accordingly, the registered β counts of the wire segments are proportional to the thermal flux they were exposed to.

In order to perform the irradiation, the wire is put into a thin plexiglass tube, which is then inserted into the specified fuel subchannel or vertical irradiation channel. After starting the reactor, the power is increased to 1 kW and maintained for 6 min. Following the irradiation, the Dy wire is first cooled for 30 min, then it is removed from the plexiglass tube, and fixed to a metal rail, which is inserted in the measuring equipment. The measuring equipment consists of a sample holder rail, movable by a stepper motor, and a stationary scintillation β-detector equipped with a collimator with a window of 5 mm width. A computer program is used to control the movement of the rail under the detector. For the measurements described in this paper, the rail was moved in steps of 5 mm length and the measurement time was set to 10 s. After the measurement, decay correction was performed on the registered data set.

The number of counts can be expressed as:

$$\begin{aligned}\varphi(\underline{r},t_w) &= \int_{t_w}^{t_w+t_m} \eta A(\underline{r},t_w)\mathrm{e}^{-\lambda t'}dt' = \frac{\eta A(\underline{r},t_w)(1-\mathrm{e}^{-\lambda t_m})\mathrm{e}^{-\lambda t_w}}{\lambda} \\ &= \Phi_{th}(\underline{r})\left\{\frac{G\overline{\sigma}_d N_d(1-\mathrm{e}^{-\lambda t_a})}{\lambda}\right\}\mathrm{e}^{-\lambda t_w}\left(1-\mathrm{e}^{-\lambda t_m}\right),\end{aligned} \tag{3}$$

where φ is the number of registered counts, η is the detector efficiency, A the sample activity, λ the decay constant of Dy-165, Φ_{th} the thermal flux, G the self-shielding factor, $\overline{\sigma}_d$ the average thermal cross section, N_d the number of Dy-164 nuclei, t_w the time interval between a fixed time (e.g. shutdown of the reactor or beginning of the measurement of the first segment) and the beginning of the measurement of the given segment, t_a the activation and t_m the measurement times.

As the geometry, activation time and measurement time are the same for each segment of the wire, by dividing each registered counts by the corresponding $\mathrm{e}^{-\lambda t_w}$ values one may obtain a quantity proportional to the thermal neutron flux.

3.4. Absolute pointwise neutron flux

The activation of gold detector foils is a standard method to obtain absolute neutron flux values. Each measurement was performed by using two gold detector foils: one wrapped between cadmium and one wrapped between aluminum plates (in what follows, the latter is called bare detector). The detector foils were fixed to a plexiglass sample holder, which was inserted into the proper vertical irradiation-channel of the reactor. The plexiglass holder was positioned so that the detectors be at the mid-height of the reactor. Once the sample was fixed, the operator started the reactor and set the power to 1 kW. The irradiation lasted 6 min. The gamma-spectrum of the samples was measured using a calibrated HPGe detector. The activities for both bare and cadmium shielded samples were obtained by Eq. 4, while the neutron flux was calculated according to Eq. 5 (Horváth, 2015). Eq. 5 contains the correction for the startup phase.

$$A = \frac{T}{t_m \eta \gamma}, \tag{4}$$

$$\Phi = A(t_2)\left[\frac{\lambda N\sigma_a}{e^{\omega t_1}(\omega+\lambda)}\left(e^{(\omega+\lambda)t_1}-1\right)e^{-\lambda(t_2+t_w)} + N\sigma_a\left(\left(1-e^{-\lambda t_2}\right)-\left(e^{\lambda t_1}-1\right)e^{-\lambda t_2}\right)e^{-\lambda t_w}\right]^{-1}, \tag{5}$$

where T is the net peak area, t_m the measurement time, η the detector efficiency, γ the gamma transition probability, ω the exponential time constant of the reactor power, t_1 the time of reaching nominal power, t_2 the end time of the measurement, while t_w is the time passed between the end of the irradiation and the beginning of the measurement.

4. Reactor physics codes and methods

The Serpent 2 Monte Carlo particle transport code was chosen for the steady-state modeling of the BME TR reactor, primarily because of its lattice physics and burnup calculation capabilities. In order to perform deterministic calculations, suitable model of the BME TR reactor were also prepared for the PARCS (diffusion), SPNDYN (diffusion and SP3 (Simplified P_3)) and PARTISN (discrete ordinates) codes.

The rest of this section briefly presents the above mentioned computer codes.

4.1. Serpent 2

Serpent 2 is a Monte Carlo reactor physics burnup calculation code developed by the VTT Technical Centre of Finland since 2004. At that time, general-purpose Monte Carlo codes were not capable of generating group constants, the predecessor of Serpent (called Probabilistic Scattering Game, or PSG) was created to fill this shortcoming (Leppänen et al., 2015a). In 2015, Serpent 2 was released which is the newest version as of today. The applications of the Serpent code range from standard reactor physics calculations (i.e. criticality calculations, fuel cycles studies, group constant generation etc.) to neutron and gamma photon transport simulations for dose rate, shielding, medical physics or even fusion related calculations. Recently, Serpent 2 was used for coupled multi-physics simulations as well (Valtavirta et al., 2017; Leppänen et al., 2015b). For the calculations of this paper, the version 2.1.31 (released in May 16, 2019) was applied.

4.2. PARCS

PARCS (Purdue Advanced Reactor Core Simulator) is a three-dimensional deterministic reactor core simulator developed originally by the Purdue University. The code solves the diffusion or the SP3 equations for steady-state and time-dependent problems in either square or hexagonal geometries. Spatial discretization can be done with either a classic coarse finite difference mesh (CMFD) or with nodal blocks as PARCS is fitted with several high-order nonlinear nodal kernels (analytic nodal method, nodal expansion method, triangular polynomial expansion nodal method etc.). High resolution pin level calculations can be performed by the fine mesh finite difference (FMFD) kernel. A separate code module called GENPMAXS was developed for processing and converting certain lattice physics code outputs (e.g. HELIOS, CASMO, Serpent etc.) to appropriate PARCS input format. The calculations presented in this paper were performed by the version 3.3.1 of PARCS and were assisted by the GENPMAXS version 6.2.

4.3. SPNDYN

SPNDYN is a three-dimensional deterministic reactor physics code developed at the Institute of Nuclear Techniques of BME (Babcsány et al., 2020; Babcsány and Kis, 2020) since 2014. The code has two main modules that are both able to solve the multi-group diffusion and SP3 equations, of which the latter can take into account up to third-order group-to-group anisotropic scattering. One of its modules – applied here for the calculations – is based on continuous Galerkin weighted residual approach as spatial discretization, while time dependence is treated by the theta finite difference method. For the finite element mesh generation, SPNDYN is applied with the GMSH open source three-dimensional mesh generator, which has a built-in CAD engine (Geuzaine et al., 2009). The other module of the code is based on hybrid finite element method and optimized to stationary hexagonal reactor problems. Both modules require a fixed-format group constant input file, hence with a small pre-processing effort SPNDYN can be used with the generally applied group constant generator codes. The SPNDYN calculations presented in this paper were performed with the code version 1.0.7.

4.4. PARTISN

The PARTISN code (Alcouffe et al., 2008) is designed to solve the steady-state or time-dependent multigroup discrete ordinates form of the Boltzmann transport equation in user-defined geometries. The code was developed at Los Alamos National Laboratory (LANL), and it is the evolutionary successor to the DANTSYS code system. PARTISN is capable of performing calculations in one, two, and even three-dimensional geometries, where the user has to define the problem in rectangular or cylindrical coordinate systems. The presented PARTISN calculations were performed with the code version 5.97.

5. Reactor physics modeling

5.1. Serpent 2 model

The Serpent model was created based on the available technical drawings and material compositions of the reactor (Klujber and Horváth, 2020). The model is cylindrical. The bottom plane is at the outer surface of the vessel (45 cm below the bottom of the fuel active length), the top plane is 75 cm above the end of the fuel active length, while the model radius is identical to the outer radius of the reactor vessel. Sensitivity calculations showed that modeling beyond the mentioned surfaces does not affect the multiplication factor significantly.

Core elements were modeled precisely with the exception of the following simplifications:

- Graphite and fuel assembly handles were omitted.
- The assembly walls were modeled square, even though they are slightly rounded at the corners.
- The truncated cone parts and the rounded edges of the fuel pin end plugs of the fuel pins were simplified.
- The rod spacers are modeled as a homogeneous aluminium-water mixture with the density adjusted to the cladding–water ratio of a regular assembly. The material used for both the regular and modified assemblies was the same.
- Each assembly is characterized by a specific fuel material, but the rods within a given assembly share the same material composition.
- Minor simplifications were made in the structure of the pneumetical rabbit system.

Based on the performed sensitivity studies, these simplifications are justified as they have minor effect on either the flux shape and spectra or the multiplication factor.

Sections of the geometry can be seen in Figs. 4 and 5 plotted by Serpent 2.

Thermal $S(\alpha, \beta)$ data for water and graphite, and continuous-energy neutron cross-section data for all materials were sampled from ENDF/B-VII.0 libraries evaluated at 300.0 K (".00t" and ".03c" extensions). Sampling from unresolved resonance probability table was switched on.

As the Serpent model is used for reference calculations and group constant generation as well, it is important to adjust the excess reactivity and the control rod worth to the measured values.

In 1981, the excess reactivity of the reactor was measured to be 1.563 $ (Zsolnay et al., 1980), while in January 2020 it was 0.693 ± 0.010 $. In order to obtain the present fuel composition, a burnup calculation was performed. Each assembly was characterized by a specific material card which shared the same material composition at the beginning. The burnup calculation was split into two sequences:

- Sequence 1: 1971–1980
  The model is consistent with the old core configuration. The energy produced in the period was evenly distributed in time for a 9 year-long burnup sequence and a year of decay sequence.
- Sequence 2: 1981–2020
  The model is reproducing the current core configuration. The energy produced in the period was evenly distributed in time for a 39 year-long burnup sequence and a year of decay sequence.

As the precise initial fuel composition and density are unknown, the isotopic vector of the fuel was taken from Table 1 and the density was adjusted uniformly such that the calculated initial excess reactivity of 1981 matches the measured value. In this way, the initial fuel density was set at 5.57 g/cm^3 (mass and diameter measurements on the spare fuel pins predicted a value of 5.63 g/cm^3, while calculations based on the nominal fuel mass and fuel dimensions gave 5.44 g/cm^3). The burnup calculation predicted 0.718 ± 0.004 $ excess reactivity in 2020, which is close to the measured value (0.693 ± 0.010 $ based on the control rod S-curves).

The uppermost position of the safety and control rods was set 5 cm above the top plane of the fuel active lengths. The diameter of the boron carbide pellets and the thickness of the cadmium

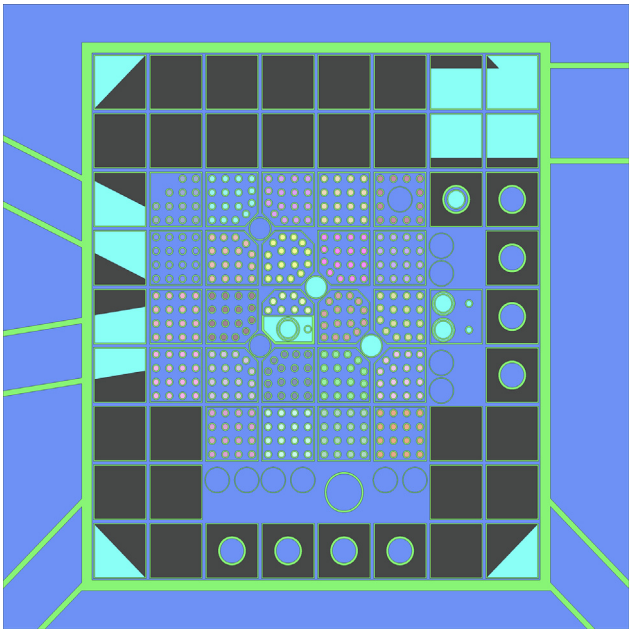

Fig. 4. Horizontal section of the reactor core at mid-height of the fuel active length (Serpent 2 model).

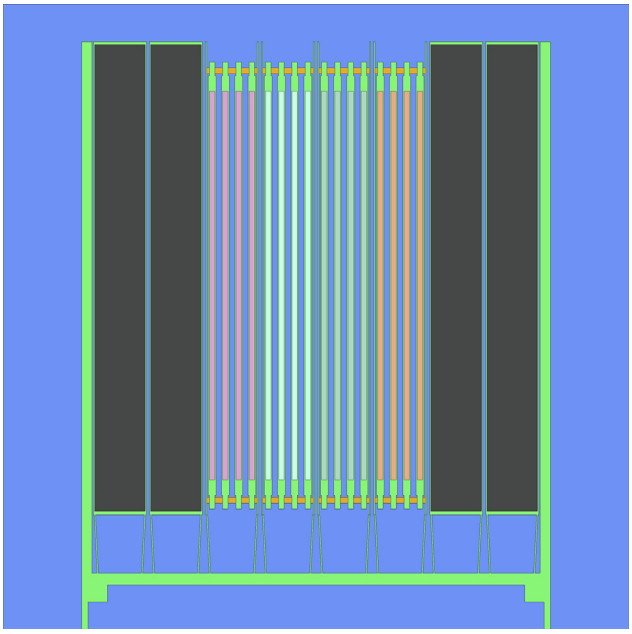

Fig. 5. Vertical view of the reactor core at the level of the seventh row (Serpent 2 model).

absorber layer were tuned so that the reactivity differences obtained by the corresponding k-eigenvalue calculations match the measured integral rod worth values within 3 ¢ (see Table 2). The measurements were performed by the rod drop method and the reactivity values were calculated by the method of inverse kinetics. The presented measurement errors only account for the counting statistics. The measurement methodology is described in subsection 3.1.

Various measured critical rod positions at zero power were used for verifying the rod reactivity worth values and axial positions (see Table 3). The measured and calculated values agree within 100 pcm, a result which can be deemed good considering the number of uncertain parameters.

Table 2
Measured and Serpent calculated integral rod worth values. Rod positions 0 mm and 600 mm correspond to fully inserted and fully withdrawn states.

Rod	Rod position(s) (mm)	Measured ($)	Calculated ($)
SR1	$z_{AUT} = 300$ mm, $z_{MAN} = 600$ mm	2.059 ± 0.013	2.068 ± 0.013
SR2	$z_{AUT} = 300$ mm, $z_{MAN} = 600$ mm	3.408 ± 0.025	3.394 ± 0.013
AUT	$z_{MAN} = 400$ mm	0.852 ± 0.002	0.875 ± 0.007
MAN	$z_{AUT} = 300$ mm	1.887 ± 0.001	1.861 ± 0.007

Table 3
Serpent calculated k-eigenvalues for measured critical rod positions.

AUT (mm)	MAN (mm)	Calculated k_{eff} (–)
180	600	0.99993 ± 0.00007
210	547	1.00025 ± 0.00007
333	450	1.00086 ± 0.00007
374	425	1.00095 ± 0.00007

The effective delayed neutron fraction of the reactor is assumed to be $7.49 \cdot 10^{-3} \pm 1 \cdot 10^{-5}$, the generation time $7.074 \cdot 10^{-5} \pm 1 \cdot 10^{-8}$ s based on Serpent 2 calculations by ("Nauchi's method Nauchi and Kameyama (2005)") method.

5.2. Group constant generation

BME TR is considered a small size (57.6 cm × 64.8 cm × 57 cm) high neutron leakage research reactor. The great number of irregularities and the many material regions present in the core makes its deterministic modeling (especially the generation of appropriate group constants) a highly challenging task.

Group constant generation for large reactors is usually carried out by deterministic lattice physics codes, which apply reflective boundary condition to the unit cell (pin or assembly) and use various leakage models as corrections (two-step approach). Serpent 2 can be utilized for such problems as well (Leppänen et al., 2016), moreover, in the case of small size reactors the full-scale geometry can be implemented in the code, giving no need for artificial leakage correction (full-core approach).

Recently, several studies dealt with the modeling of research reactors using the Serpent 2 code for reference calculations beside few-group constant generation and diffusion codes for further analysis (Rais et al., 2017; Siefman et al., 2015; Fejt and Frybort, 2018; Shchurovskaya et al., 2020). The following conclusions can be highlighted:

- The use of Serpent 2 as lattice physics code for diffusion calculation group constant generation is advantageous in the case of small size reactors.
- The effective multiplication factors calculated by diffusion codes using two energy groups tend to have a deviation larger than 1000 pcm from the reference values. This is mainly attributed to the diffusion coefficient generation. By default, Serpent uses the so-called out-scatter approximation, which is inaccurate in light-water reactors due to the scattering anisotropy of hydrogen.
- Transport cross section correction (TRC) for hydrogen introduced by Herman et al. (2013) was tested and found to be an effective method to reduce the error of the multiplication factor below 500 pcm.

Several full-core homogenization schemes were tested for BME TR to obtain the best configuration which can be used with diffusion codes as well. The quality of each scheme was evaluated by comparing the excess reactivity, the power distribution and the

control rod worth values calculated by PARCS using transport correction with the Serpent reference solution.

Various homogenization schemes were investigated. First, all of the fuel assemblies were divided vertically into quarters and each of these parts, along with the water region surrounding the core, were treated as separate materials ($72 \times 4 + 1$ regions). Diffusion calculations yielded a deviation of more than 400 pcm from the reference value of the manual control rod worth, which indicated that the unit cell size of the homogenization may have been too small.

The unit cell size was increased and, as a next step, each assembly was homogenized separately ($72 + 1$ regions). The excess reactivity and the integral rod worth values matched the reference ones within 100 pcm, while the maximum relative error of the assembly power distribution remained below 5% when transport correction was applied.

Finally, as a last attempt to improve the control rod worth values, the absorbers were homogenized in the four surrounding assemblies, while for the rest of the core the unit cell size remained unchanged ($66 + 1$ regions). Nevertheless, both the excess reactivity and the rod worth values showed larger deviations from the reference ones than in the previous case.

Based on the diffusion calculation results, the second approach was chosen for further calculations. Group constant sets were generated in 2, 4, 14 and 40 groups using the pre-defined CASMO group structures of Serpent. The generated two-group constants are provided along with this paper in text file format.

Nodal diffusion codes are usually fitted to utilize surface and assembly discontinuity factors (ADF, introduced by Smith in 1980 (Smith, 1980)) which adjust the neutron current at the surfaces of different homogenized regions.

Sets of ADFs were generated with Serpent exclusively for the PARCS model. The subsequent diffusion calculation results showed significant improvement in terms of both differential quantities and power distribution as well. Nevertheless, to draw more general conclusions, especially using ADFs and TRC together, further investigations are needed and a more thorough discussion is thus deferred to a separate work.

5.3. PARCS model

Diffusion calculations were realized with the PARCS code (version 3.3.1). The Serpent generated group constants were processed by the GENPMAXS code (version 5.97). The nodal geometry consisted of a 0.5 m high 22×23 square lattice of moderator and fuel assemblies (assembly pitch: 7.2 cm) bordered by a 0.5 m high 22×23 square lattice of moderator reflector regions from the bottom and the top (see Fig. 6). At the boundaries, a zero flux condition was applied. For each calculation the so-called hybrid nodal kernel of PARCS was applied. The hybrid kernel uses the analytic nodal method with the exception of cases when there is no net leakage out of a node; then it applies the Nodal Expansion Method. In each case the excess reactivity, control rod worth and assembly worth values were calculated using the appropriate Serpent generated group constant libraries. A mesh independent solution was found with 4 radial and 10 axial divisions within a node. Each PARCS calculation was carried out with a two energy group approximation, without (PARCS 2G) and with TRC correction (PARCS 2G TRC). The correction curve used in the diffusion calculations is the same as that obtained by Herman in Herman et al. (2013).

5.4. SPNDYN model

With the aim of code-to-code comparison, similarly to the geometric model applied for the PARCS calculations, a GMSH-based

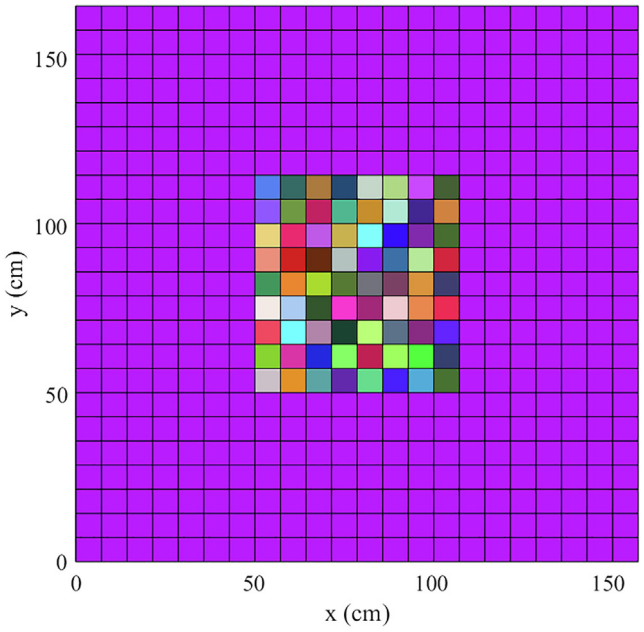

Fig. 6. Radial segment of the geometry used for the deterministic calculations.

CAD model of the 0.5 m high 8×9 square (7.2 cm $\times$ 7.2 cm) assemblies and the surrounding 0.5 m reflector region in each direction was prepared. Taking advantage of the symmetry to the axial mid-plane, the CAD model was reduced to the half geometry from $z = 0$ m to $z = 0.75$ m along with prescribing reflective boundary condition on the $z = 0.75$ m plane. On the other boundaries, in the case of diffusion calculations – similarly to the PARCS model – a zero flux boundary condition was adopted, while for the SP3 calculations, Marshak vacuum boundary condition was used. For each calculation to be done, a preliminary study was performed to select an appropriate unstructured and non-uniform mesh (an example of which is shown in Fig. 7). For excess reactivity and integral rod worth calculations, a mesh with 33265 nodes was applied. The worth of the graphite reflectors (B2, C2, D2, E2) and of the outer (B3, C3, B4) and inner (C4) fuel assemblies was calculated with a mesh with 42456, 132080 and 393470 nodes, respectively, as these parameters were found to be more sensitive to mesh refinement. Finally, the 132080-node mesh was also used to calculate the power distribution. Two-group constants generated using Serpent were applied for all of the diffusion and SP3 calculations. Diffusion calculations were performed without and with the introduction of transport cross section correction for hydrogen (SPNDYN 2G DIFF and SPNDYN 2G DIFF TRC), while in the case of SP3 calculations the following approaches were considered:

- the effective diffusion coefficient matrix D1 is considered to be equal to the diagonal matrix of the diffusion coefficients without transport cross section correction corresponding to the usual practice of applying approximate and only linearly anisotropic group-to-group scattering by using the transport cross section within SP3 calculations (Duerigen, 2013) (SPNDYN 2G SP3 DIFFCOEF);
- the D1 effective diffusion coefficient matrix is considered to be equal to the diagonal matrix of the diffusion coefficients with transport cross section correction allowing the consideration of hydrogen-induced anisotropic scattering (SPNDYN 2G SP3 DIFFCOEF TRC);
- the effective diffusion coefficient matrices (D1 and D2) are calculated according to their original definition from the total cross section and the linearly and third-order anisotropic scattering

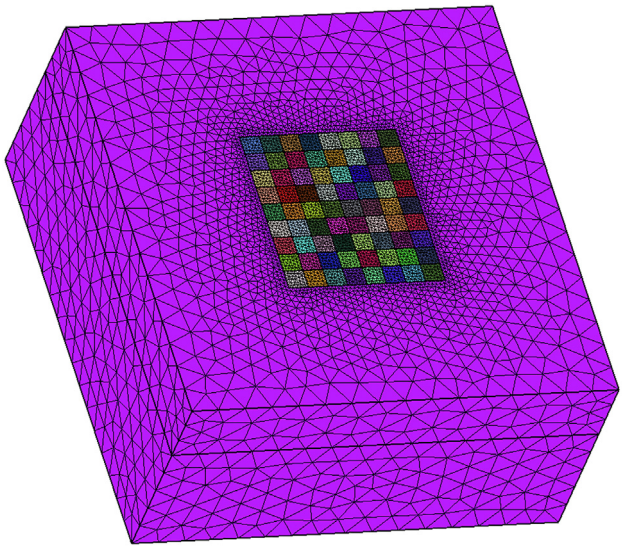

Fig. 7. An example of the unstructured and non-uniform meshes applied for the SPNDYN calculations.

matrices (see Eq. (12) and (13) in Babcsány and Kis (2020)). For this approach four-group and fourteen-group calculations were carried out as well (SPNDYN 2G/4G/14G SP3).

5.5. PARTISN model

In order to compare the results to a transport solution, the PARTISN neutron transport solver was chosen. Prior to the current model, another geometric description and group constant set was already used for the modeling of BME TR with the ERANOS code for transport simulation purposes (Böröczki et al., 2020). The model contained smaller heterogeneous regions which were more suitable for transport approximation. Both steady-state and transient calculations were carried out. The same Serpent-generated group constant libraries were applied as in the PARCS and SPNDYN calculations, and the geometric description of the 0.5 m high 8×9 square lattice of assemblies surrounded by reflector region was used. As for the SPNDYN model, the axial symmetry of the geometry was taken into account and a reflective boundary condition was applied on the half-height plane. A mesh independence test was performed for several different cases and a subdivision of each assembly region into $10 \times 10 \times 25$ nodes was found to be appropriate. For the reflector region 25 divisions were chosen along all the three axes. Due to the large leakage of the reactor, the higher-order scattering matrices had a significant effect on the effective multiplication factor. Therefore, a scattering anisotropy up to the third order was adopted for the simulations. A sensitivity study was performed for different quadrature sets and, as a result, the default TWOTRAN quadrature set with S10 order was applied. Previous experiences showed that the transport simulations with two-group libraries tend to produce higher effective multiplication factor, so the calculations were repeated in a few cases for 4, 14 and 40 groups as well.

6. Calculation and measurement comparison

6.1. Excess reactivity

In Serpent, excess reactivity was calculated with all the control rods being withdrawn. For deterministic calculations corresponding group constant libraries were generated. Table 4 presents the calculation results in pcm. The measured value was converted to pcm using the Serpent calculated β_{eff}.

Regarding the code-to-code comparison for the diffusion calculations, the PARCS and SPNDYN results are in good agreement, the difference being less than 30 pcm in both cases. The transport correction (TRC) significantly improves the excess reactivity values producing a deviation of 91 pcm and 62 pcm from the Serpent reference value. Compared to the non-corrected diffusion results, the SP3 calculations provide better agreement when approximate linearly anisotropic group-to-group scattering is applied by using the diffusion coefficient without transport cross section correction. However, the SP3 calculations with both transport cross section corrected diffusion coefficients and original D1 and D2 effective diffusion coefficient matrix definitions highly overestimate the effective multiplication factor, resulting in a significantly overestimated excess reactivity (584 pcm and 6442 pcm, respectively). The transport calculations performed with PARTISN significantly overestimate the excess reactivity for 2, 4, 14 and 40 energy groups as well. By increasing the number of energy groups for both the PARTISN and the SPNDYN SP3 calculations, however, the values seem to converge towards the Serpent solution. The PARTISN and SPNDYN SP3 results (for the latter, using the original effective diffusion coefficient definition) differ by 90 pcm, 160 pcm and 274 pcm for 2, 4 and 14 energy groups, respectively, which can be regarded as a good agreement.

The primary cause of the large deviations experienced with the transport codes PARTISN and SPNDYN in SP3 mode using the original effective diffusion coefficient matrix definitions is most probably related to the use of the Serpent-generated higher-order anisotropic scattering matrices. As already pointed out by Cai in Cai (2014), although Serpent can generate higher-order anisotropic scattering matrices up to the seventh order, no thorough verification and validation of their applicability in higher-order deterministic transport codes was performed so far. The higher-order anisotropic scattering matrices of Serpent are generated by using the multi-group angular deviation probability distribution function, which, however, is weighted by the scalar flux spectrum for the energy group condensation, rather than by the associated angular flux moment spectrum (see Eqs. (9)–(14) in Leppänen et al. (2016)). The inappropriate weighting of the multi-group angular deviation probability distribution function indirectly results in biased multi-group higher-order anisotropic scattering matrices. This assumption is also confirmed by the findings of Lin and Yang (2020). They concluded that the use of scalar flux weighted anisotropic scattering cross sections generated by Serpent may not be adequate for fast reactor applications where anisotropic scattering plays an important role.

The presumption of the questionable applicability of the Serpent-generated higher-order scattering matrices is also supported by the fact that running SPNDYN in SP3 mode with diffusion coefficients (either with or without TRC) as D1 instead of applying the theoretical definition of effective diffusion coefficient matrices ensures the reproducibility of the Serpent reference results with an accuracy that is in line with or slightly better than diffusion theory.

The effects of inappropriate weighting was investigated by deriving the weighting functions from the angular flux moments calculated from one of the 40 energy group PARTISN simulations. The obtained weighting functions (see Fig. 8) show significant differences between different moments, upon which inappropriate weighting may result in biased higher-order scattering matrices. The magnitude of this bias may become more significant for smaller energy group structures since the energy integration range applied during group constant generation is larger and the spectral differences result in more relevant differences in the scattering matrices. This suggests that more reliable results could be obtained with increased number of energy groups with the Serpent gener-

Table 4
Measurement-to-code and code-to-code comparison of the excess reactivity.

	$\rho_{excess}(pcm)$
Measurement	519 ± 8
Serpent	538 ± 3
PARCS 2G	−1522
PARCS 2G TRC	629
SPNDYN 2G DIFF	−1551
SPNDYN 2G DIFF TRC	600
SPNDYN 2G SP3 DIFFCOEF	−940
SPNDYN 2G SP3 DIFFCOEF TRC	1122
SPNDYN 2G SP3	6980
SPNDYN 4G SP3	2695
SPNDYN 14G SP3	1759
PARTISN 2G	7070
PARTISN 4G	2855
PARTISN 14G	2033
PARTISN 40G	1386

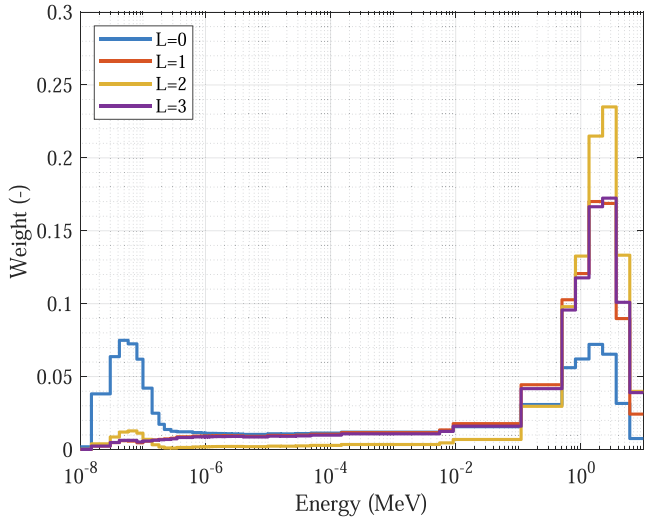

Fig. 8. Volume integrated weighting functions for the different orders for assembly F5.

ated group constants. This last conclusion is also supported by the calculation results of this paper.

6.2. Integral control rod worth

As discussed in Section 5, the integral control rod worth of the Serpent model was adjusted to the measurements. Therefore, in this subsection only code-to-code comparison is presented.

Group constant sets were generated for all four control rod configurations (AUT inserted and withdrawn, MAN inserted and withdrawn). Table 5 presents the calculation results.

The code-to-code comparison shows that PARCS and SPNDYN two-group diffusion effective multiplication factors agree well in all cases with an average absolute difference of 26 pcm. The SP3 calculations yielded an average of 594 pcm improvement in k_{eff} compared to the diffusion calculations with respect to the reference Serpent results when diffusion coefficients without TRC were considered, and an overestimation with an absolute average of 642 pcm compared to the Serpent results when diffusion coefficients with TRC were applied. Regarding the integral rod worth of the automatic control rod, there is negligible difference between the diffusion and SP3 results when diffusion coefficients either with or without TRC were applied. For both automatic and manual control rod reactivity worth, diffusion and SP3 calculations with transport cross section corrected diffusion coefficients yielded slightly worse results compared to the calculations without TRC. By using the original effective diffusion coefficient matrix definitions for the 2G SP3 calculations, however, the calculated integral rod worth values deteriorated significantly yielding a 117 pcm difference for the automatic and 124 pcm for the manual rod from the Serpent reference. The same effect with the same magnitude could be observed with the two-group PARTISN calculations (deviations of 111 pcm and 126 pcm for the automatic and manual control rods, respectively). By increasing the number of energy groups, these differences decrease but remain relatively high (81 pcm for the automatic and 56 pcm for the manual control rods) even for forty-group calculations.

6.3. Assembly worth

Two-group cross section sets were generated for nine reactor configurations (the reference state with $z_{AUT} = 430$ mm, $z_{MAN} = 400$ mm and eight states, one for each assembly worth to be calculated). All graphite reflector unit and fuel assembly worth calculations presented in Table 6 were performed making use of these group constant sets. The measured values were converted to pcm using the Serpent calculated β_{eff}.

The Serpent results differ with an absolute average of approximately 40 pcm from the measured assembly reactivity worth, with 4 pcm being the smallest and 71 pcm the largest deviation.

With regard to the code-to-code comparison, PARCS and SPNDYN results agree very well with each other as for the eight cases considered, the difference is ranging from 10 to 30 pcm. The application of Herman transport corrected diffusion coefficients for both diffusion and SP3 calculation resulted in an absolute average of about 125–150 pcm improvement compared to either the Serpent calculated or the measured reference values when the assembly C4 is not considered.

Large differences in the multiplication factors were observed when calculating the worth of the C4 fuel assembly with both diffusion and diffusion coefficient-based SP3 calculation. In these cases no improvement was experienced with the application of transport correction. The origin of these discrepancies is not yet known and need further investigation.

Taking the Serpent solution as reference and considering all deterministic cases, the best results have been provided by the SPNDYN 2G SP3 DIFFCOEF TRC method with a deviation ranging from 32 to 61 pcm in case of the graphite assemblies and from 6 to 46 pcm in case of the fuel assemblies (here the C4 case, affected by a 272 pcm deviation, was not taken into account).

Taking the Serpent solution as reference and considering all deterministic cases, the best absolute assembly worth differences were obtained with the SPNDYN 2G SP3 DIFFCOEF TRC method which yielded an absolute average difference of 46 pcm for the graphite assemblies and 69 pcm if all eight assemblies are considered.

The SPNDYN SP3 2G and PARTISN 2G calculated results agree within an average of 10 pcm. However, these results deviate significantly (27 to 102 pcm for the graphite and 185 to 376 pcm for the graphite assemblies) from the Serpent solution.

6.4. Power distribution

No measurement were performed to obtain the assembly power distribution of the core yet,[1] thus, in this subsection only a code-to-code comparison is presented.

The Serpent reference distribution was obtained by use of the *set cpd* card, while PARCS calculates axially averaged assembly dis-

[1] Thermal measurements of such purpose are already scheduled for the near future.

Table 5
Code-to-code comparison of the calculated multiplication factors and control rod worth.

Code	AUT in	AUT out	MAN in	MAN out	AUT worth (pcm)	MAN worth (pcm)
Serpent	0.99565	1.00221	0.98813	1.00208	−657	−1409
PARCS 2G	0.97592	0.98175	0.96938	0.98209	−608	−1335
PARCS 2G TRC	0.99707	1.00294	0.99020	1.00339	−587	−1328
SPNDYN 2G DIFF	0.97568	0.98147	0.96913	0.98182	−605	−1334
SPNDYN 2G DIFF TRC	0.99682	1.00265	0.98996	1.00312	−583	−1325
SPNDYN 2G SP3 DIFFCOEF	0.98157	0.98747	0.97504	0.98777	−609	−1322
SPNDYN 2G SP3 DIFFCOEF TRC	1.00209	1.00800	0.99523	1.00841	−585	−1313
SPNDYN 2G SP3	1.06515	1.07132	1.05741	1.07197	−541	−1285
SPNDYN 4G SP3	1.01822	1.02407	1.01080	1.02476	−561	−1348
PARTISN 2G	1.06611	1.07236	1.05839	1.07296	−547	−1283
PARTISN 4G	1.01979	1.02576	1.01247	1.02641	−571	−1341
PARTISN 14G	1.01120	1.01716	1.00400	1.01778	−579	−1349
PARTISN 40G	1.00464	1.01049	0.99747	1.01111	−576	−1352

Table 6
Measurement-to-code and code-to-code comparison of assembly reactivity worth.

Reactivity worth (pcm)	B2	C2	D2	E2	B3	C3	B4	C4
Measurement	232 ± 1	393 ± 2	469 ± 3	371 ± 2	1047 ± 7	1955 ± 15	1756 ± 13	3034 ± 30
Serpent	259 ± 8	443 ± 8	516 ± 8	416 ± 8	1085 ± 8	2026 ± 8	1760 ± 8	3054 ± 8
PARCS 2G	431	651	737	621	1291	2243	1997	2986
PARCS 2G TRC	343	523	598	500	1140	2027	1805	2843
SPNDYN 2G DIFF	421	633	717	604	1276	2213	1969	2958
SPNDYN 2G DIFF TRC	334	507	581	487	1125	1999	1777	2814
SPNDYN 2G SP3 DIFFCOEF	403	605	676	576	1271	2185	1951	2919
SPNDYN 2G SP3 DIFFCOEF TRC	320	487	548	464	1126	1980	1766	2782
SPNDYN 2G SP3	226	363	414	343	887	1714	1537	2678
PARTISN 2G	232	373	425	353	900	1709	1526	2689

tribution by default. For SPNDYN and PARTISN, the distributions had to be derived manually. In these cases to obtain the power distribution for each assembly (p_i), the volume integrated group scalar flux (Φ_i^g) was first multiplied by the corresponding kappa value (κ_i^g) and the fission cross section ($\Sigma_{f,i}^g$), then it was summed over all the energy groups and divided by the average power of all the fuel assemblies, i.e.:

$$p_i = \frac{\sum_{g=1}^{G} \kappa_i^g \Sigma_{f,i}^g \Phi_i^g}{\frac{1}{24}\sum_{i=1}^{24}\sum_{g=1}^{G} \kappa_i^g \Sigma_{f,i}^g \Phi_i^g} \tag{6}$$

The $z_{AUT} = 430$ mm, $z_{MAN} = 400$ mm case was chosen as a reference. Fig. 9 shows the Serpent reference solution, while Figs. 10–19 present the $(x - x_{ref})/x_{ref} \cdot 100$ relative deviation (%) of each case from the Serpent solution. Table 7 summarizes the average and the maximum deviations for each case.

With respect to the Serpent reference solution, the diffusion calculations performed with the PARCS and SPNDYN codes, without the application of TRC correction, resulted in a maximum difference of 6.35% and 6.09% and an absolute average of 2.24% and 2.33%, respectively. When transport correction was considered, the maximum differences decreased to 4.10% and 4.56%, while the absolute average deviations went down to 1.68% and 1.78%, respectively. The SPNDYN and PARCS diffusion results are in good agreement with an absolute average difference of less than 0.2% and a maximum absolute difference lower than 0.5% (see Fig. 20). Considering the SPNDYN SP3 results, there is a slight improvement compared to diffusion results if diffusion coefficients without TRC correction are applied, yielding a maximum relative difference of 5.10% and an absolute average of 2.18%; however, the SP3 power distribution is almost identical to the diffusion-based one when transport-corrected diffusion coefficients are considered. An outlying relative difference was obtained for the F3

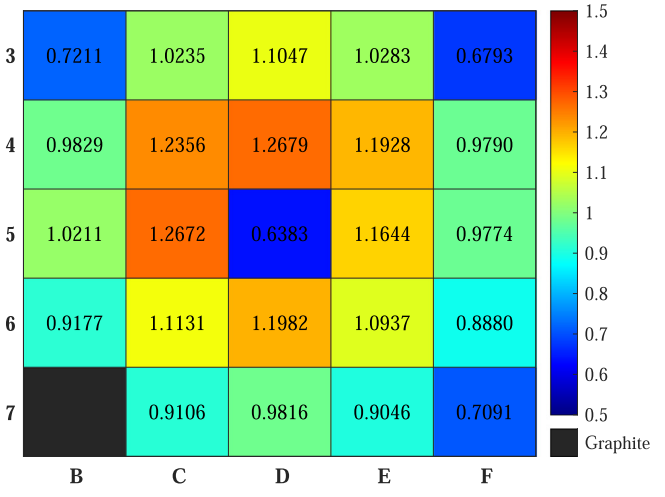

Fig. 9. Relative assembly power distribution calculated by Serpent. The standard deviation is 0.0001 for each assembly.

Table 7
Average and maxiumum relative difference between the assembly power calculated with deterministic codes and Serpent.

Code	Average (%)	Maximum (%)
PARCS 2G	2.24	6.35
PARCS 2G TRC	1.68	4.10
SPNDYN 2G DIFF	2.33	6.09
SPNDYN 2G DIFF TRC	1.78	4.56
SPNDYN 2G SP3 DIFFCOEF	2.18	5.10
SPNDYN 2G SP3 DIFFCOEF TRC	1.76	4.61
SPNDYN 2G SP3	1.61	7.55
SPNDYN 4G SP3	1.09	4.93
PARTISN 2G	1.33	6.59
PARTISN 40G	1.04	3.81

assembly with the SPNDYN 2G SP3 model (7.55%), but the average relative difference improved, resulting in an absolute average of 1.61%. By increasing the number of groups to 4 (SPNDYN 4G SP3) both the maximum and the absolute average difference decreased significantly to 4.93% and 1.09%, respectively. Two-group PARTISN calculations yielded an average 1.33% and a maximum of 6.59% deviation from the Serpent reference. The outlying value of 6.59% corresponds to the more thermal F3 assembly as it was the case with the SP3 calculations. By increasing the number of energy groups, the average deviation decreased to 1.04%, while the maximum to 3.81%.

6.5. Axial thermal neutron flux distribution

In the case of the deterministic calculations the heterogeneous neutron flux was not reconstructed, thus, in this subsection only a comparison between the Serpent results and the measured values is presented.

Using Serpent, the axial flux distribution was tallied with the *det* card. In each subchannel the tallied volume was $0.4 \times 0.4 \times 100$ cm^3. To actually simulate the measurements, a tally multiplier for Dy capture was used. The calculated distributions were first normalized then plotted against the decay-corrected measured raw data (see Figs. 22–29 in Appendix B). The bottom end of the measured curves deviate from the Serpent results: it drops to zero due to the termination of the Dy-wire. Due to this effect and the uncertainty of the measurement–calculation fitting, the axial uncertainty of the measured points is estimated of about 3 mm. The uncertainty of the detected counts (due to Poisson statistics, positioning, collimator geometry etc.) is estimated to be about 0.03 in relative units. The curves are generally in good agreement, however, the measured and calculated reflector hump heights differ in some cases, a difference which can probably be attributed to unknown local geometric irregularities or material inhomogeneities.

6.6. Pointwise thermal neutron flux

Similarly to the axial thermal neutron flux distributions, pointwise thermal neutron flux comparison is only presented between measurements and Serpent calculations.

The pointwise flux was tallied with Serpent through the use of the *det* card. The tallied volumes were in all cases $0.4 \times 0.4 \times 0.4$ cm^3 cubes situated in the axial mid-plane of the reactor. To best simulate the measurements, a tally multiplier for Au-197 capture was used and only neutrons with energies below 0.5 eV (Cd cutoff energy) were tallied. To eliminate the uncertainty of the reactor power[2] from the comparison, all the measured and calculated data were normalized with respect to the average of the measured values and the calculated values, respectively (see Table 8).

The average relative difference of the measured and calculated data is 8.4% while the maximum is 24.3%. The values of the calculated-to-experimental ratios (C/E) deviate symmetrically from 1 (the standard deviation is 0.11, the skewness is 0.76), thus no special dependence or bias is observed. Given that gold activator foil measurements have a relative error of about 5% the obtained results are in acceptable agreement.

[2] The reactor power of BME TR is based on the calibration of neutron detectors to thermal flux measurements, which were done several decades ago; in the near future, a recalibration procedure will be performed.

Table 8
Measurement to Serpent comparison of pointwise thermal neutron flux values.

Channel	Measurement (–)	Serpent 2 (–)	C/E (–)
C8	1.55 ± 0.08	1.34 ± 0.01	0.87 ± 0.04
C9	0.61 ± 0.03	0.58 ± 0.01	0.95 ± 0.05
D6	1.36 ± 0.07	1.35 ± 0.01	0.99 ± 0.05
D9	0.68 ± 0.03	0.61 ± 0.01	0.88 ± 0.05
E8	1.38 ± 0.07	1.39 ± 0.01	1.01 ± 0.05
E9	0.62 ± 0.03	0.56 ± 0.01	0.91 ± 0.05
F8	1.27 ± 0.06	1.27 ± 0.01	0.99 ± 0.05
F9	0.47 ± 0.02	0.48 ± 0.01	1.02 ± 0.06
G4	1.33 ± 0.07	1.48 ± 0.01	1.11 ± 0.06
G6	1.39 ± 0.07	1.57 ± 0.01	1.13 ± 0.06
H4	0.79 ± 0.04	0.70 ± 0.01	0.88 ± 0.05
H6	0.54 ± 0.03	0.67 ± 0.01	1.24 ± 0.06

7. Conclusions and summary

In this paper, the authors presented steady-state reactor physics measurements and comprehensive numerical analysis performed for the Training Reactor of Budapest University of Technology and Economics.

Measurements were carried out to obtain excess reactivity, integral control rod worth, fuel assembly and graphite reflector unit worth values. Using the activation method, relative axial thermal neutron flux distributions were measured in assembly subchannels and pointwise thermal neutron flux values were determined in various mid-plane positions of the reactor.

Based on the available technical drawings and material composition tables, BME TR was modeled with the Serpent 2 state-of-the-art Monte Carlo particle transport code. The unknown parameters such as the exact control rod compositions have been adjusted to the results of rod worth measurements. The obtained Serpent model was used for group constant generation which have been then used for deterministic simulations.

Calculations were performed by the Monte Carlo code Serpent 2, diffusion code PARCS, diffusion and SP3 code SPNDYN and discrete ordinates code PARTISN to obtain excess reactivity, integral control rod worth, fuel and graphite assembly worth, relative assembly power distribution, pointwise thermal neutron flux values and axial thermal neutron flux distributions at various reactor positions.

The developed Serpent model was validated against measurements that were not used for model adjustments. The calculated fuel assembly and graphite reflector block reactivity worth values differ with an absolute average of 40 pcm from the measurements. The calculated axial thermal neutron flux distributions are in generally good agreement with the measured curves, while most of the pointwise thermal neutron flux C/E ratios match the calculations within about two standard deviations.

It has been repeatedly demonstrated that the Serpent-generated group constants can be applied with high fidelity both for diffusion and SP3 calculations if the D1 effective diffusion coefficient matrix is considered to be equal to the diagonal matrix of the diffusion coefficients in an SP3 code. However, transport calculations involving higher-order scattering matrix elements yielded inaccurate results for differential reactivity values and absolute multiplication factors as well. Based on the findings in the open literature, the comparison with the SP3 results and the analysis of higher-order moment spectra, the highlighted problems are most probably due to the inappropriate scalar flux weighting of the higher-order moments, which leads to inconsistent higher-order anisotropic scattering matrix generation by Serpent.

It was found that the application of TRC transport correction introduced by Herman is generally advantageous for both diffusion and SP3 calculations regarding absolute multiplication factors, dif-

ferential reactivity values and power distribution as well. In the case of control rod worth and one of the assembly worth calculations, the TRC correction, even though improved the multiplication factors, did not improve the corresponding reactivity worth.

Taking the Serpent solution as reference and considering all the calculations performed, the TRC corrected PARCS nodal diffusion calculations yielded for the multiplication factors an absolute average difference of 81 pcm, an absolute average difference of 79 pcm regarding the reactivity worth and an absolute average deviation of 1.68% in terms of assembly power distribution. Given the small size and the high-leakage property of the investigated reactor, the results are already considered a good basis for future transient and multi-physics calculations.

Future work will consist of further development of the PARCS diffusion model of BME TR by the application of appropriate discontinuity factors and the realization of the two-step group constant generation approach. Transient neutronic and thermal measurements are also planned for BME TR in the near future.

Declaration of Competing Interest

The authors declare that they have no known competing financial interests or personal relationships that could have appeared to influence the work reported in this paper.

Acknowledgements

The authors would like to express their gratitude to the members of the Reactor Operation Group and the Guard and Radiation Protection Service of BME TR who provided constant and invaluable help in the realization of the measurements presented in this paper.

The research reported in this paper was supported by the BME NC TKP2020 grant of NKFIH Hungary.

This work has been partially supported by the ENEN+ project that has received funding from the Euratom research and training Work Programme 2016-2017-1#755576.

Appendix A. Relative assembly power distributions

Figs. 10–21.

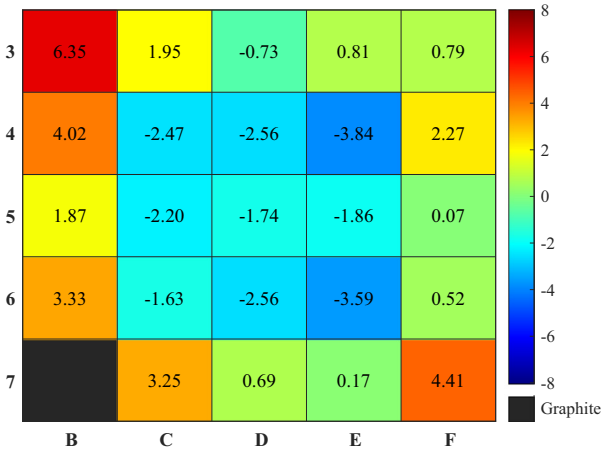

Fig. 10. Relative difference between the assembly powers calculated with PARCS 2G and Serpent.

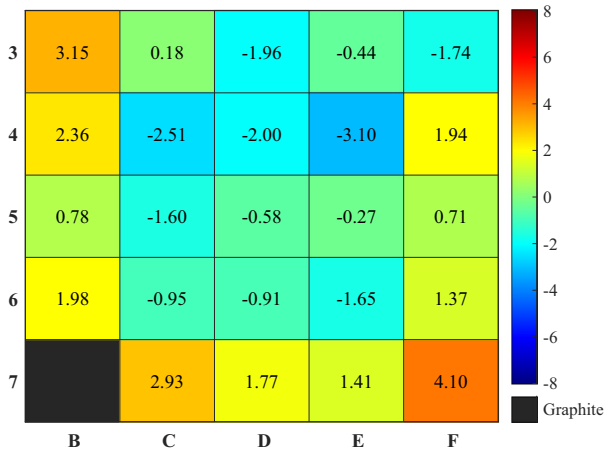

Fig. 11. Relative difference between the assembly powers calculated with PARCS 2G TRC and Serpent.

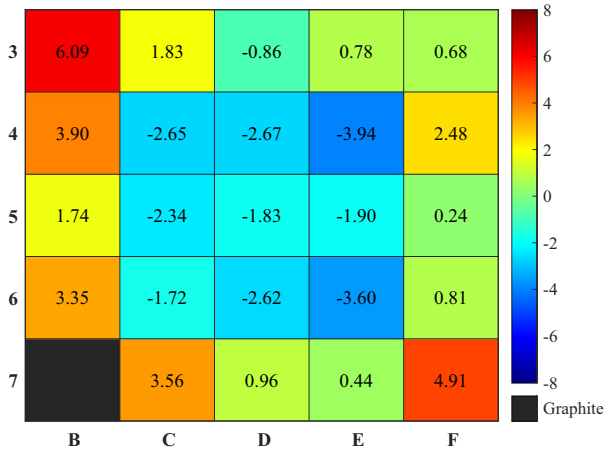

Fig. 12. Relative difference between the assembly powers calculated with SPNDYN 2G DIFF and Serpent.

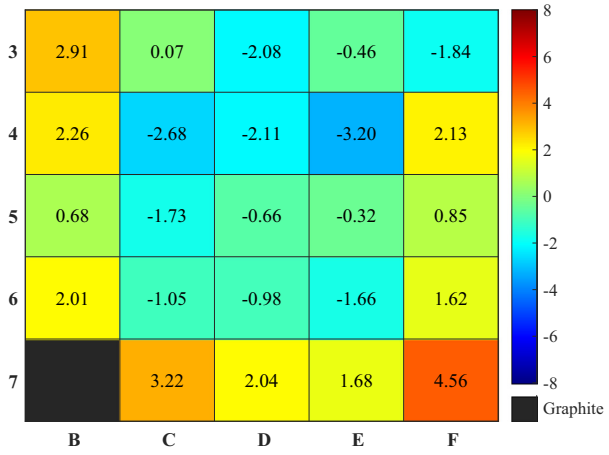

Fig. 13. Relative difference between the assembly powers calculated with SPNDYN 2G DIFF TRC and Serpent.

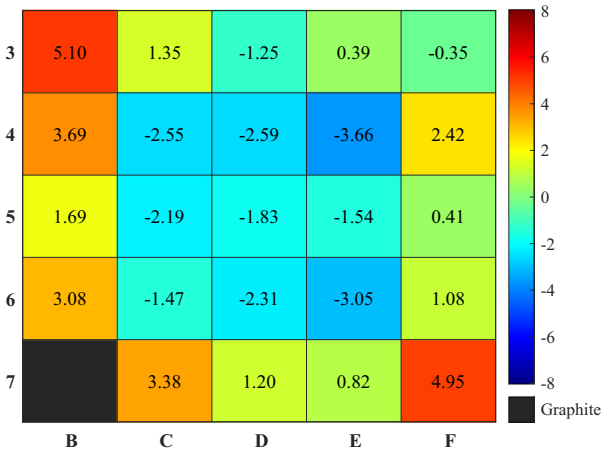

Fig. 14. Relative difference between the assembly powers calculated with SPNDYN 2G SP3 DIFFCOEF and Serpent.

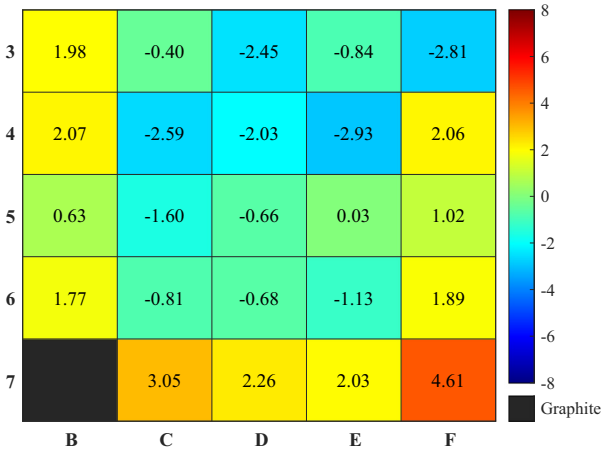

Fig. 15. Relative difference between the assembly powers calculated with SPNDYN 2G SP3 DIFFCOEF TRC and Serpent.

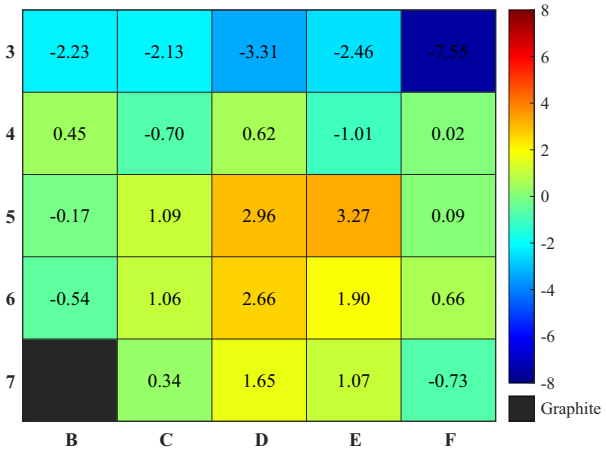

Fig. 16. Relative difference between the assembly powers calculated with SPNDYN 2G SP3 and Serpent.

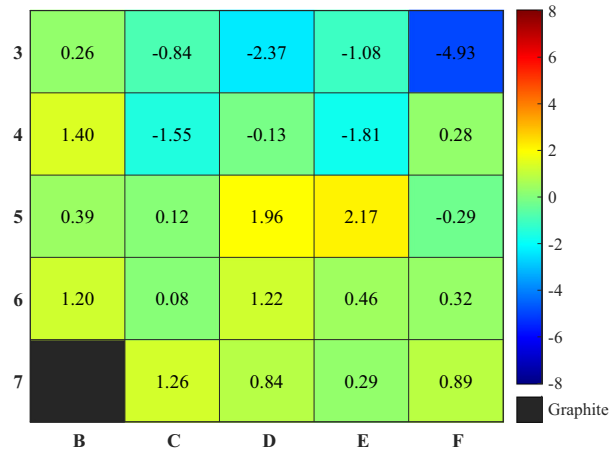

Fig. 17. Relative difference between the assembly powers calculated with SPNDYN 4G SP3 and Serpent.

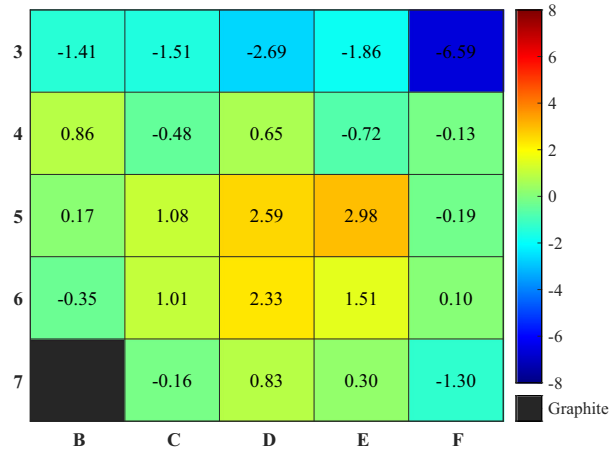

Fig. 18. Relative difference between the assembly powers calculated with PARTISN 2G and Serpent.

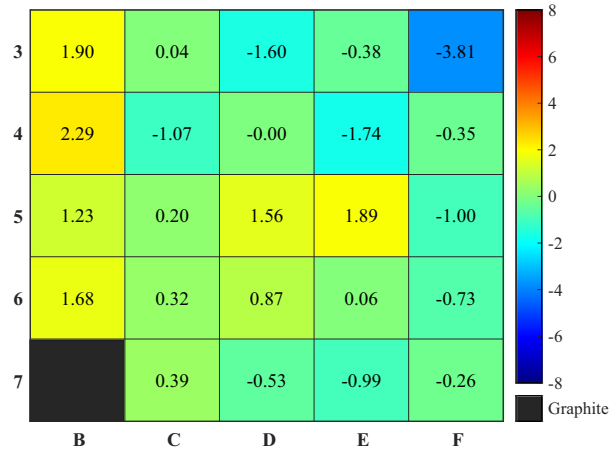

Fig. 19. Relative difference between the assembly powers calculated with PARTISN 40G and Serpent.

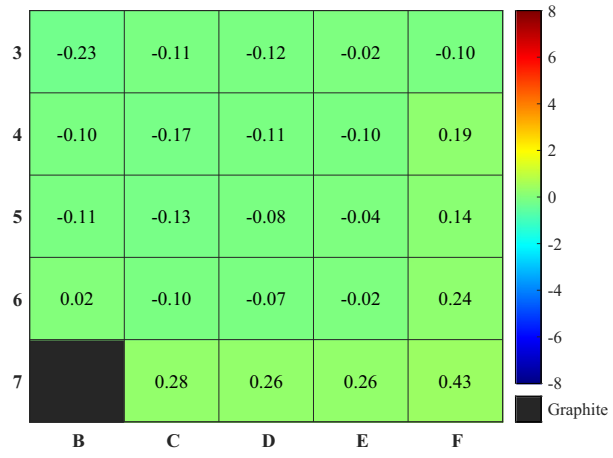

Fig. 20. Relative difference between the assembly powers calculated with PARCS 2G TRC and SPNDYN 2G TRC.

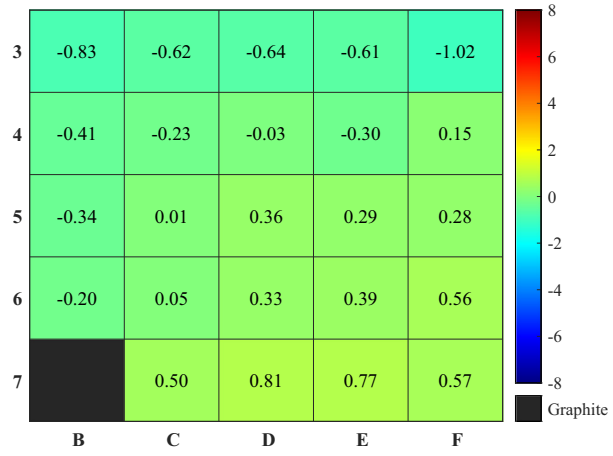

Fig. 21. Relative difference between the assembly powers calculated with SPNDYN 2G SP3 and PARTISN 2G.

Appendix B. Axial thermal neutron flux distribution

Figs. 22–29.

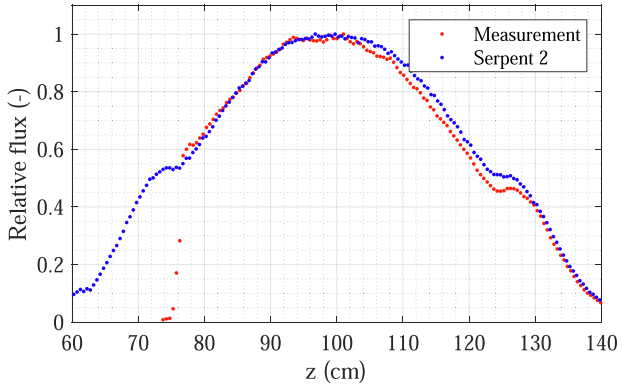

Fig. 22. Relative thermal neutron flux distribution in fuel subchannel B3/1.

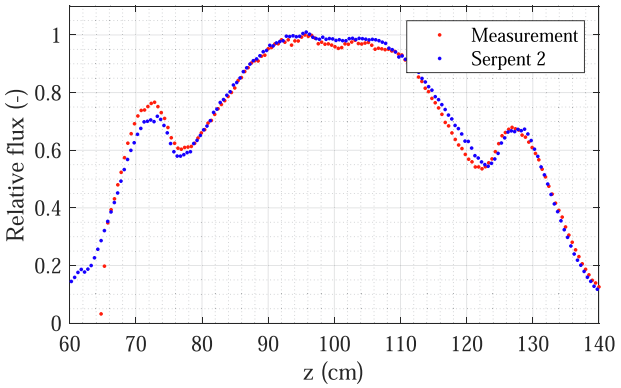

Fig. 23. Relative thermal neutron flux distribution in fuel subchannel B4/1.

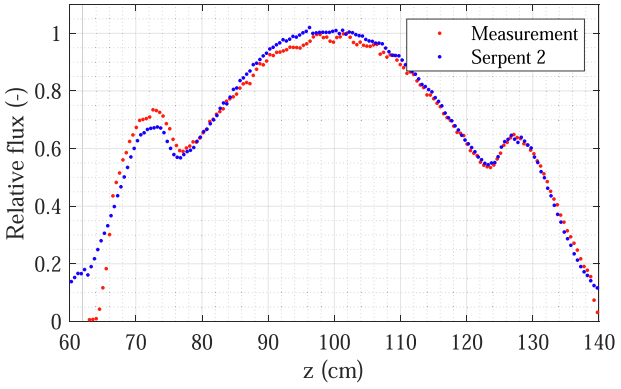

Fig. 24. Relative thermal neutron flux distribution in fuel subchannel B6/7.

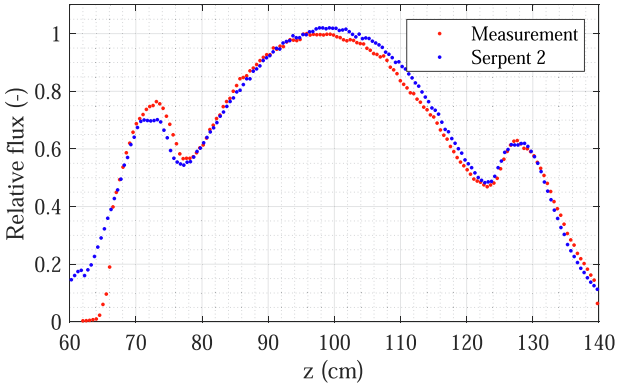

Fig. 25. Relative thermal neutron flux distribution in fuel subchannel C6/9.

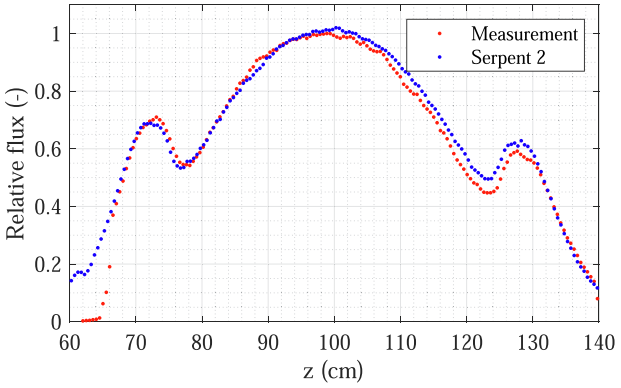

Fig. 26. Relative thermal neutron flux distribution in fuel subchannel D6/9.

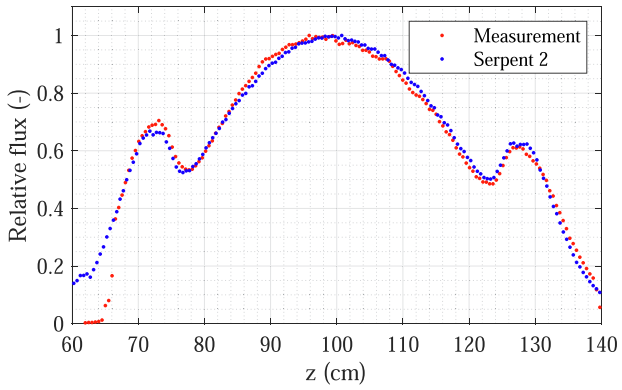

Fig. 27. Relative thermal neutron flux distribution in fuel subchannel E3/9.

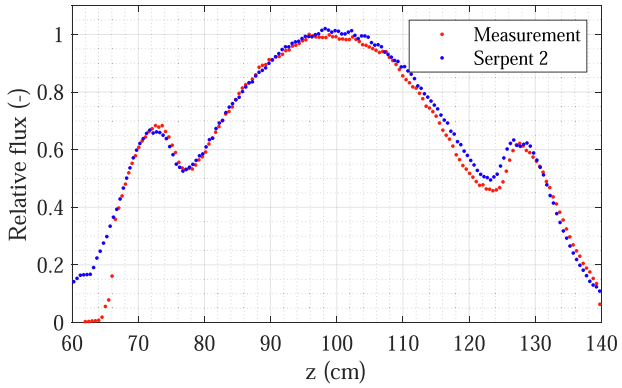

Fig. 28. Relative thermal neutron flux distribution in fuel subchannel E7/1.

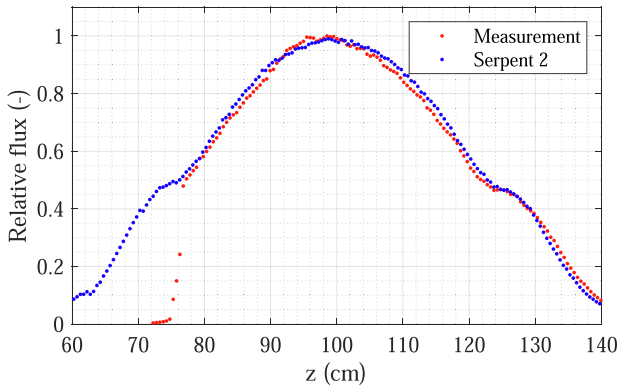

Fig. 29. Relative thermal neutron flux distribution in channel F3.

References

Rhoades, W.A., Childs, R.L., 1991. TORT: a three-dimensional discrete ordinates neutron/photon transport code. Nucl. Sci. Eng. 107, 397.

Grundmann, U., Rohde, U., 1996. DYN3D – A 3-dimensional core model for steady state and transient analysis in Thermal reactors. In: Proc. Int. Conf. On the Physics of Reactors "PHYSOR 96", Mito (Japan)..

Gaston, D., Newman, C., Hansen, G., Lebrun-Grandié, D., MOOSE, 2009. A parallel computational framework for coupled systems of nonlinear equations. Nucl. Eng. Des. 239, 1768–1778.

Fiorina, C., Clifford, I., Aufiero, M., Mikityuk, K., 2015. GeN-Foam: a novel OpenFOAM based multi-physics solver for 2D/3D transient analysis of nuclear reactors. Nucl. Eng. Des. 294, 24–37.

Schmidt, R., Belcourt, K., Hooper, R., Pawlowski, R., Clarno, K., Simunovic, S., Slattery, S., Turner, J., Palmtag, S., 2015. An approach for coupled-code multiphysics core simulations from a common input. Ann. Nucl. Energy 84, 140–152.

Csom, Gy., Kovács, M., Aszódi, A., 2020. http://www.reak.bme.hu/en/training-reactor.html.

Szatmáry, Z., Horváth, A., 2018. Final Safety Report for BME TR, volume 4 (in Hungarian). .

Budapest Neutron Centre, 2020. http://www.bnc.hu. .

Duderstadt, J.J., Hamilton, L.J.,1976. In: Nuclear Reactor Analysis, John Wiley & Sons, Chap. 6, p. 270.

LND 23210 Boron lined neutron proportional counter – https://www.lndinc.com/products/neutron-detectors/23210, (2020)..

Horváth, A., 2015. Reactor physics measurements on the Training Reactor (in Hungarian), Annex to the Final Safety Report for BME TR. .

Leppönen, J., Pusa, M., Viitanen, T., Valtavirta, V., Kaltiaisenaho, T., 2015a. The Serpent Monte Carlo code: status, development and applications in 2013. Ann. Nucl. Energy, 82, pp. 142–150.

Valtavirta, V., Leppänen, J., Viitanen, T., 2017. Coupled neutronics–fuel behavior calculations in steady state using the Serpent 2 Monte Carlo code. Ann. Nucl. Energy 100, 50–64.

Leppänen, J., Hovi, V., Ikonen, T., Kurki, J., Pusa, M., Valtavirta, V., Viitanen, T., 2015b. The numerical multi-physics project (NUMPS) at VTT Technical Research Centre of Finland. Ann. Nucl. Energy 84, 55–62.

Babcsány, B., Bartók, T., Kis, D.P., 2020. Finite element solution of the time-dependent SP3 equations using an implicit integration scheme. Kerntechnik 85, 292–300.

Babcsány, B., Kis, D.P., 2020. Semi-analytical methods for SP3 equations solver verification including third-order scattering anisotropy. Ann. Nucl. Energy 148, 107671.

Geuzaine, C., Remacle, J.-F., 2009. GMSH: a three-dimensional finite element mesh generator with built-in pre- and post-processing facilities. Int. J. Numer. Methods Eng. 79.

Alcouffe, R.E., Baker, R.S., Dahl, J.A., Turner, S.A., Ward, R.C., 2008. PARTISN: A Time-Dependent, Parallel Neutral Particle Transport Code System, Tech. Rep. LA-UR-08-07258 (Los Alamos National Laboratory) .

Klujber, G., Horváth, A., 2020. Benchmark description of the BME Training Reactor. BME-NTI-854/2018, version 3.0. .

Zsolnay, É., Csom, Gy., Szondi, E., Lévai, F., 1980. Initial measurements on the converted core of BME TR (in Hungarian). Research report..

Nauchi, Y., Kameyama, T., 2005. Proposal of direct calculation of kinetic parameters β_{eff} and Λ based on continuous energy Monte Carlo method. J. Nucl. Sci. Technol. 42, 503–513.

Leppänen, J., Pusa, M., Fridman, E., 2016. Overview of methodology for spatial homogenization in the Serpent 2 Monte Carlo code. Ann. Nucl. Energy 96, 126–136.

Rais, A., Siefman, D., Hursin, M., Ward, A., Pautz, A., 2017. Neutronics modeling of the CROCUS reactor with SERPENT and PARCS codes. In: International Conference on Mathematics and Computational Methods Applied to Nuclear Science and Engineering April 16–20, 2017. Jeju, Korea.

Siefman, D.J., Girardin, G., Rais, A., Pautz, A., Hursin, M., 2015. Full Core modeling techniques for research reactors with irregular geometries using Serpent and PARCS applied to the CROCUS reactor. Ann. Nucl. Energy 85, 434–443.

Fejt, F., Frybort, J., 2018. Analysis of a small-scale reactor core with PARCS/Serpent. Ann. Nucl. Energy 117, 25–31.

Shchurovskaya, M.V., Geraskin, N.I., Kruglikov, A.E., 2020. Comparison of research reactor full-core diffusion calculations with few-group cross sections generated using Serpent and MCU-PTR. Ann. Nucl. Energy 141, 107361.

Herman, B.R., Forget, B., Smith, K., Aviles, B.N., 2013. Improved diffusion coefficients generated from Monte Carlo codes, Tech. Rep., American Nuclear Society, 555 North Kensington Avenue, La Grange Park, IL 60526 (United States). .

Smith, K.S., 1980. Spatial homogenization methods for light water reactor analysis. PhD Dissertation, Massachusetts Institute of Technology, Deptartment of Nuclear Engineering, https://dspace.mit.edu/handle/1721.1/16042.

Duerigen, S., 2013. Neutron transport in hexagonal reactor cores modeled by trigonal-geometry diffusion and simplified P3 nodal methods. PhD Dissertation, Karlsruhe Institute of Technology, https://www.osti.gov/etdeweb/servlets/purl/22230894 .

Böröczki, Z.I., Klujber, G., Tolnai, G., Molnár, B., Légrády, D., Gabrielli, F., Rineiski, A., Szieberth, M., 2020. Simulation of a research reactor reactivity transient with deterministic and GPU-assisted Monte Carlo reactor kinetics codes. Eur. Phys. J. Plus 135.

Cai, L., 2014. Condensation and homogenization of cross sections for the deterministic transport codes with Monte Carlo method: Application to the GEN IV fast neutron reactors. PhD Dissertation, Université Paris Sud – Paris XI, English, NNT: 2014PA112280, tel-01126922.

Lin, C.-S., Yang, W.S., 2020. An assessment of the applicability of multigroup cross sections generated with Monte Carlo method for fast reactor analysis. Nucl. Eng. Technol.